Asian Journal of Pharmaceutical Sciences 15 (2020) 69–82

Available online at www.sciencedirect.com

ScienceDirect

journal homepage: www.elsevier.com/locate/AJPS

Original Research Paper

Redox-sensitive, PEG-shielded carboxymethyl PEI nanogels silencing MicroRNA-21, sensitizes resistant ovarian cancer cells to cisplatin

Sanaz Javanmardi[a], *Ali Mohammad Tamaddon*[b,c], *Mahmoud Reza Aghamaali*[a,*], *Ladan Ghahramani*[b], *Samira Sadat Abolmaali*[b,c,**]

[a] *Department of Biology, Faculty of Science, University of Guilan, Rasht 64891, Iran*
[b] *Center for Nanotechnology in Drug Delivery, Shiraz University of Medical Sciences, Shiraz 71345, Iran*
[c] *School of Pharmacy, Shiraz University of Medical Sciences, Shiraz 71345, Iran*

ARTICLE INFO

Article history:
Received 27 July 2018
Revised 4 October 2018
Accepted 29 October 2018
Available online 1 December 2018

Keywords:
MicroRNA
PEI nanogels
Anti-miR-21
Gene delivery
Cisplatin resistance

ABSTRACT

A series of branched polyethylenimine (PEI) modifications including PEGylation (PEG2k-PEI) for steric shielding, redox-sensitive crosslinking for synthesis PEG2k-PEI-ss nanogels and subsequent carboxymethylation (PEG2k-CMPEI-ss) for modulation of the polymer pk_a have been introduced for cellular delivery of Anti-miR-21. The synthesis was characterized using ^1H NMR, FTIR, TNBS, potentiometric titration, particle size and ζ potential. Loading of Anti-miR-21 at various N/P ratios was investigated by gel retardation, ethidium bromide dye exclusion, heparin sulfate competition and DNase I digestion experiments. The miR-21 silencing was measured by stem-loop RT PCR in A2780 ovarian cancer cell lines whether it is sensitive to resistant to cisplatin. It has been shown that PEG2k-CMPEI-ss was well suited for delivery of Anti-miR-21 in terms of nucleic acid loading, preservation against extracellular matrix and nucleases and sequence-specific silencing of miRNA-21 *in vitro*. Moreover, it has been demonstrated that pre-treating cells with Anti-miR-21 loaded nanogels can sensitize them to cis-Pt even at non-toxic concentraions. The results indicate that PEG2k-CMPEI-ss mediated microRNA delivery can be considered as a novel strategy for ovarian cancer therapy.

* Corresponding author. Department of Biology, Faculty of Science, University of Guilan, Rasht 64891, Iran.
** Corresponding author. Department of Pharmaceutical Nanotechnology and Center for Nanotechnology in Drug Delivery, Shiraz University of Medical Sciences, Shiraz 71345, Iran. Tel.: +98 71 32424127.
E-mail addresses: aghamaali@guilan.ac.ir (M. Aghamaali), abolmaali@sums.ac.ir (S. Abolmaali).
Peer review under responsibility of Shenyang Pharmaceutical University.

https://doi.org/10.1016/j.ajps.2018.10.006

1. Introduction

Ovarian cancer is the 6th most common cancer in women [1]. Major risk factors contributing to increase ovarian cancer have been mentioned as hereditary, reproductive, hormonal, inflammatory, dietary and surgical [2]. Indeed, it has been reported that hormone replacement therapy can be considered as the major risk factor for developing ovarian cancer [3]. Regarding that only 30% of ovarian cancer patients at advanced stages can survive only 5 years after initial diagnosis [4], so urgent needs for developing new therapeutic strategies seem to be undeniable.

For almost 40 years, cisplatin (cis-Pt) has been the most accepted drug for treating ovarian cancer. It has been reported that 80%−90% of patients with ovarian cancer respond to platinum chemotherapy, however nearly about one third of them resist to cis-Pt [5]. Various mechanisms of cis-Pt resistance have been studied which can be divided into pump (mediated by P-glycoprotein and multi-drug resistance proteins) and non-pump mechanisms which are mainly due to anti-apoptotic cellular defense activations mediated by Bcl-2 and survivin [6,7]. Cis-Pt resistance can also occur by elevating metallothioneins and glutathione content of the cells. In addition, increasing DNA repair can be considered as an antiapoptotic factor in cis-Pt resistant cells [8].

MicroRNAs (miRNAs), non-coding endogenous evolutionarily conserved ~18–22 nucleotide single-stranded RNAs, were discovered in 1993 [9]. It has been clear that miRNAs have major roles in gene expression regulation through base pair formation with messenger RNAs [8]. miRNAs biogenesis and their mechanisms of action have been well studied and it has been demonstrated that any changes in intracellular amounts of miRNA lead to severe diseases including autoimmune malfunctions [10], diabetes [11], Parkinson's [12], fibrosis [13] and cardiovascular [14] abnormalities and cancers such as breast, glioblastoma, liver, ovary, prostate, lung, gastric, colon, and endocrine pancreatic tumors [15].

MicroRNA-21 (miR-21) has been considered as an oncogenic miRNA that upregulates in almost all diseases, downregulates tumor inhibitor proteins, leads to cell proliferation, migration, invasion, metastasis, and apoptosis regulation [16]. Several studies demonstrate that miR-21 overexpression leads to downregulation of critical tumor inhibitor proteins such as phosphatase and tensin homolog (PTEN), programmed cell death protein 4 (PDCD4), hypoxia inducible factor–1α (HIF-1α) and regulates drug resistance in ovary cancer cells [17–21]. So, delivery of Anti-miR-21 to ovarian cancer cells seems to be a promising way to inhibit tumor cell proliferation and metastasis.

It has been reported that upregulation of miR-21 in ovarian cancer is responsible for cis-Pt resistance in cancer cells by PDCD4 upregulation *via* JNK-1/c-Jun/miR-21 pathway [22]. The most important challenge to achieve convenient therapeutic approaches for miR/anti-miR therapy is lack of suitable delivery system which can overcome the obstacles of systemic delivery such as phagocytic elimination, renal filtration, nucleases degradation, cellular uptake and endosomal release for possible translation to clinical practices [23,24].

PEIs have wide applications for gene delivery because of their controlled polycationic nature which allow them to condense negatively charged oligonucleotide chains, protect them against nucleases and facilitate nucleic acid entering efficiently *via* endocytosis [25,26]. Moreover, PEIs increase endosomal escape attributed to the well-known proton sponge mechanism [27,28]. Chemical modifications of PEI primary and secondary amines can enhance endosomal release of genetic materials by decreasing pKa that makes the modified polymer more protonable at acidic than neutral pH [29,30]. In addition, it has been shown that addition of carboxyl groups induces proton sponge effect since ionized carboxylate groups serve as proton-acceptors and enhanced buffer capacity of nanovectors [31]. Also, the nanogels composed of PEG-PEI can effectively deliver drug or oligonucleotide due to the positively charged core of PEI and the shell of mPEG which leads to solubility enhancement, rapid endosomal uptake, prevention of unwanted interactions of particles with plasma components and nuclease protection [32–34]. In addition, these sterically stabilized nanoscale particles can easily provide a convenient environment for encapsulation of negatively charged biological agents such as miRNAs to promote their resistance against changes in pH, ionic strength and solvent [33,35]. Simultaneously, biodegradable crosslinking provides the demanded stability of a relatively new generation of nanovectors, also called nanogels, that causes protection of loaded oligonucleotide chains. Furthermore, redox-sensitive disulfide linkages facilitate their breaking down and intracellular release of encapsulated contents in presence of glutathione and reducing enzymes of the cells, but prevent pre-mature release and degradation in the extracellular milieu [34–37].

In this regard, we aimed to synthesis a series of branched PEI modifications including PEGylation reaction (PEG2k-PEI) for steric shielding, redox-sensitive chemical crosslinking (PEG2k-PEI-ss) for nanogel preparation and subsequent carboxymethylation reaction (PEG2k-CMPEI-ss) for modulation of the polymer pk_a, respectively. To investigate the possible role of disulfide crosslinks and the carboxymethylation reaction, the physicochemical and biological properties of the nanogels were compared in terms of loading Anti-miR-21, formation of stable nanoplexes, cellular delivery and transfection efficiency. In addition, the therapeutic value of Anti-miR-21 loaded PEG2k-PEI-ss nanogels was compared in A2780 sensitive (A2780S) and resistant (A2780R) cell lines to cis-Pt.

2. Materials and methods

2.1. Chemical

Polyethyleneimine 10 kDa (corresponding to M_w/M_n of 1.4) and methoxy polyethylene glycol 2 kDa ($mPEG_{2000}$–COOH) were purchased from Poly Sciences Inc. (Canada) and Jenkem (USA), respectively. Dithiodipropionic acid (DTDP), 1-(3-dimethylamino-propyl)-3-ethylcarbodiimide hydrochloride (EDC), N-hydroxysuccinimide (NHS), 2,4,6-trinitrobenzene sulfonic acid (TNBS), disodium ethylenediaminetetraacetic acid (EDTA), agarose, 4,6-diamidino-2-phenylindole (DAPI), fluorescein isothiocyanate (FITC), sodium borohydride ($NaBH_4$), 4-morpholineethanesulfonic acid (MES), cisplatin (cis-Pt)

and 3-(4,5-dimethyl-thiazol-2-yl)-2,5-diphenyltetrazolium bromide (MTT) were supplied from Sigma-Aldrich (USA). $ZnSO_4.7H_2O$, dichloromethane (DCM), dimethylsulfoxide (DMSO), triethylamine (TEA), ethidium bromide (EtBr) and potassium bromide (KBr) were obtained from Merck (Germany). A2780S and A2780R ovarian cancer cell lines were purchased from Pasteur Institute (Iran, Tehran). Anti-miR-21, scrambled and primer sequences were synthesized by Macrogen (Korea).

2.2. Synthesis of PEG2k-PEI-ss nanogels

Coordination complex, micellar template-assisted synthesis and characterization of PEG2k-PEI-ss was carried out according to the previous method by Abolmaali et al. [33,38]. Briefly, a solution of NHS-activated $mPEG_{2000}$–COOH in methanol was added to PEI solution in DCM at $mPEG_{2000}$/PEI weight ratios at 0.5. The medium was supplemented by 1% TEA as a proton quencher and the tubes were incubated for 3 h while stirring. The product was concentrated using a rotational speed vacuum (Christ RVC 2–18, Germany), diluted in 3 ml of deionized water, dialyzed using a Float-A-Lyzer 6–8 kDa (Spectrum, USA) and lyophilized (Christ alpha 1–2 LD, Germany). For the crosslinking reaction, 30 mg of PEG2k-PEI dissolved in 100 mM MES buffer pH 5.6, $ZnSO_4$ solution was added dropwise to the polymer solution (Zn^{2+}/N ratio = 0.2) and stirred 30 min to constitute a micellar template for the crosslinking reaction. The crosslinking reaction was done by adding100 mM DTDP solution in DMSO, EDC and NHS, at the molar ratio of 2:2:1 (NHS/EDC/COOH). The mixture was stirred overnight and then the coordinated Zn^{2+} was removed by dialysis against HCl solution (pH 3.0) using Float-A-Lyzer 3.5 kDa.

2.3. Carboxymethylation reaction

To carboxylate PEI primary and secondary amines buried in the core of PEG2k-PEI-ss nanogels, a solution of 12 mg bromoacetic acid in 3 ml DMSO was added dropwise to 4 ml nanogels (2.5 mg/ml). The product (PEG2k-CMPEI-ss) was then stirred overnight at room temperature and then dialysis in double distilled water for 3 d and stored in 4 °C before use.

2.4. Characterization of the nanogels

2.4.1. TNBS assay

To calculate the amount of residual primary amines in PEG2k-PEI copolymer, PEG2k-PEI-ss and PEG2k-CMPEI-ss nanogels, TNBS assay was performed according to the method described by Freedman and Radda [39] at polymer concentrations equal to 0.75 mM PEI. To 0.5 ml of each standard and sample solutions diluted in 0.1 M borate buffer (pH = 9.5), 2.6 µl TNBS reagent was added. Following 45 min incubation at 25 °C, the absorbance was read at $\lambda = 420$ nm using UV–visible spectrophotometer (ELISA reader, Biotek, USA).

2.4.2. FTIR spectroscopy

Infrared spectra were recorded on FTIR spectrometer (Vertex, Bruker, Germany) to study spectral changes. Samples were prepared by geometric dilution of an identical amount of the lyophilized products with KBr and compression of the mixtures to form discs. Twenty scans were signal averaged with a resolution of 4 cm^{-1} in range of 500–4000 cm^{-1}.

2.4.3. ^1H NMR

^1H NMR spectra was recorded on Bruker-400 MHz using D_2O as solvent. Proton integration method was used to estimate average degree of PEGylation, disulfide crosslinking and carboxymethylation.

2.4.4. Potentiometric titration

The potentiometric titration was performed to estimate the degree of carboxymethylation. Briefly, aliquots of 20 µl of 1 M NaOH solution were added to solutions of PEG2k-PEI, PEG2k-PEI-ss and PEG2k-CMPEI-ss nanogels (equals to 1 mg PEI). Each mixture was titrated with aliquots of 0.5 M HCl while shaking at 25 °C. The titration curves were plotted and compared for the nanogels.

2.4.5. Ellman assay

To determine the redox-sensitivity of the nanogels, either simple or carboxylated, Ellman assay was performed [40]. Briefly, 25 µl of the reagent (0.2 M $NaBH_4$ in 0.2% NaOH solution) were mixed to 45 µl of samples containing 4 mM total amines and incubated for 1 h. The volume reached to 90 µl with 300 mM HEPES buffer (pH 8). Then, 10 µl of 4 mg/ml DTNB solution (Ellman's reagent) was added. After 15 min incubation, the absorbance was read at 412 nm. The free thiol content was calculated using a calibration curve plotted for reduced glutathione standard solutions.

2.5. Preparation and characterization of Anti-miR-21 loaded nanogels

2.5.1. Gel retardation assay

Nanoplexes were prepared by simple mixing of Anti-miR-21 or scramble sequences with PEG2k-PEI copolymer, PEG2k-PEI-ss and PEG2k-CMPEI-ss nanogels at various N/P ratios ranging from 0 to 10 in deionized water. The products were further incubated for 0.5, 3, 6 and 24 h at room temperature. Nanoplexes were run in Bio-Rad electrophoresis apparatus at 60 V, 30 min in 2.5% (w/v) agarose gel and visualized by UV transilluminator (Syngene gel documentation system) [41].

2.5.2. Ethidium bromide (EtBr) dye exclusion assay

EtBr dye exclusion assay was performed to determine the optimum N/P ratio for loading and condensation of nucleic acid sequences [42]. Nanoplexes were prepared according to the aforementioned method in 96-well plates. After 30 min incubation at room temperature, 50 µl of 0.5 µg/ml of EtBr solution was added to each sample and mixed gently. The mixtures were incubated in dark condition for 15 min and the fluorescence intensity was read at excitation and emission $\lambda = 510$ nm and $\lambda = 595$ nm, respectively. Naked Anti-miR-21 sequence and deionized water were considered as positive and negative controls, respectively.

2.5.3. Heparin sulfate competition assay

To investigate stability of the Anti-miR-21 loaded nanoplexes against heparin sulfate (extracellular polyanion), agarose

gel electrophoresis was performed. In this condition, the nanoplexes were prepared at various N/P molar ratios and the mixtures were incubated for 24 h at room temperature. Then, 2 μl of heparin sulfate (2 U/μg oligonucleotide) was added to each sample, pipetted several times and after 15 min incubation, they were run in 2.5% agarose gel at 60 V for 30 min. The bands were visualized using Syngene gel documentation apparatus. In parallel, biological stability of the nanoplexes was investigated by measuring their resistance against heparin sulfate by the EtBr dye exclusion assay. Briefly, 0.1–2 IU heparin sulfate/μg oligonucleotide sequences were added to each well of 96-well plate containing nanoplexes. After 15 min incubation, 50 μl of 1 μg/ml EtBr was added to each well. Fluorescence intensities were determined before and after addition of heparin sulfate as mentioned before and any change in nucleic acid condensation (%) were calculated accordingly.

2.5.4. *Stability of nanoplexes against DNaseI*

To investigate the biological stability of nanoplexes against nucleases, the nanoplexes at the N/P = 5 and also 3 μg of naked Anti-miR-21 were mixed with 2 μl of reaction buffer and 2 U of DNaseI, separately. The mixtures were incubated at 37 °C for different times (0 min, 1, 3, 6 and 24 h). Aliquots at different incubation times were run in 2.5% agarose gel electrophoresis and their stability against DNaseI was compared to naked Anti-miR-21 [43].

2.5.5. *Determination of particle size and ζ potential*

Particle size was investigated by the dynamic light scattering spectrometry (DLS 180°, Microtrac, Germany) using a patented controlled reference method which incorporates 180° heterodyne detection by calculating signals of various scattered light frequencies combined with the reflected signals of un-shifted frequency of the original laser (780 nm) to generate a wide spectrum of frequencies. The power spectrum of Doppler frequency shifts was then applied for the multimodal and broad size distribution measurements. The hydrodynamic diameters of the nanogels and their respective nanoplexes with Anti-miR-21 were determined in 20 mM phosphate buffer (pH = 7) at the effective N/P molar ratio = 5. The viscosity and refractive index of water at 25 °C were used for data analysis. The intensity averaged diameters were reported for each sample. To calculate ζ potentials, the diluted samples underwent analysis by calibrated Zeta-check (Microtrac, Germany) for oscillating zeta streaming potential.

2.6. *Cell culture*

Cellular studies were carried out using A2780S and A2780R ovarian cancer lines. The cells were cultured in RPMI medium supplemented with 10% fetal bovine serum (FBS; PAA, Australia) and 1% antibiotic (Penicillin–Streptomycin, Australia) in an incubator at 37 °C and 5% CO_2. In order to preserve the resistance phenotype, aliquots of 0.1 μM cis-Pt was added to A2780 drug resistance cell line after each passage.

2.6.1. *MTT cytotoxicity assay*

A cell count of 2.5×10^4 A2780R and A2780S cells was seeded in 96-well plates. After 24 h incubation at 37 °C and 5% CO_2, the cells were treated with the culture medium containing various concentrations of PEG2k-PEI copolymer, PEG2k-PEI-ss and PEG2k-CMPEI-ss nanogels, at the concentrations ranged between 0 and 100 μg/ml, to evaluate cytotoxicity of the polymeric biomaterials. Furthermore, the MTT assay was performed to investigate the sequence specific cytotoxicity associated with Anti-miR-21 *vs.* scrambled sequence (100 ng/ml) loaded with the nanogels at different N/P mole ratios (1, 3, 5) for 72 h. The medium was replaced with 100 μl MTT (0.5 mg/ml) in PBS and incubated for a further 3 h. Finally, the medium was aspirated and the remaining formazan crystals were solubilized in 100 μl/well DMSO. Light absorbance was measured at 570 nm and corrected for the background absorbance at 650 nm. Cell viability was calculated as percentage relative to untreated control cells [44].

2.6.2. *Trypan blue membrane leakage assay*

A2780R and A2780S cells were seeded (10^6 cells/well) in 6-well plates. After 24 h, the cells were incubated with solutions of the polymers alone, PEG2k-PEI, PEG2k-PEI-ss and PEG2k-CMPEI-ss nanogels at the concentration of 32 mg/l, or the loaded nanoplexes prepared at the constant N/P = 5 (3 μg/l Anti-miR-21 or the scrambled sequence). Next, the cells were trypsinized and suspended in PBS containing trypan blue and counted to determine the percentage of viable cells (with clear cytoplasm) *vs.* non-viable cells (blue stained cytoplasm). Cell membrane leakage was expressed as the percentage of non-viable to total cells. Untreated cells served as control [45].

2.6.3. *Cellular uptake and intracellular release by fluorescence microscopy*

Cellular uptake of the FITC-labeled nanogels was determined by fluorescence microscopy. First, to label the nanogels, 200 μl of 10 mg/ml FITC was added to 4 ml of the nanogels (1.3 mg/ml) in 0.1 M borate buffer (pH 9.2) and the mixture was incubated for 2 h stirring. The excess FITC was removed by dialysis using Float-A-Lyzer (8–10 kDa) at 4 °C in dark. The degree of conjugation was determined using standard curve plotted for FITC at λ = 495 nm. Then, 10^5 cells (A2780R and A2780S) were seeded in 6-well plates and treated for 0.5, 2 and 4 h with either 50 μg/ml FITC-labeled nanogels. Following treatment, the cells were washed with cold PBS and fixed with 2% paraformaldehyde in PBS at 37 °C for 10 min. After washing with cold PBS, the cells were permeabilized with Triton X-100 (0.5% in PBS) for 10 min at 4 °C and washed with cold PBS. The nuclei were stained with DAPI solution (10 μg/ml in PBS) for 5 min before visualized by the fluorescence microscope (Nikon Eclipse E400, Japan).

2.6.4. *miR-21 expression assay by stem-loop RT PCR*

After 24 h incubation of the seeded cells in 6-well plates, the cells were treated by nanoplexes with N/P = 5 molar ratios for 72 h. Then, the cells were scrapped and total RNA was extracted according to Dena Zist Asia Kit procedure. cDNA synthesis was done using M-MuLV-Reverse Transcriptase and special stem-loop primer for microRNA-21 (30 min 16 °C, 60 min 42 °C followed by 10 min 70 °C). Polymerase chain reaction (PCR) was done with the following pattern: 94 °C for 2 min, followed by 40–60 cycles of 93 °C for 30 s, 58 °C for 1 min

and 72 °C for 30 s. The products were run on 2.5% agarose gel at 60 V for 30 min. Results were analyzed by ImageJ software.

2.7. *Interaction between miR-21 downregulation and cis-Pt resistance*

In order to evaluate the effect of treating cells with Anti-miR-21 loaded nanoparticles on cis-Pt action, the sensitive and resistant cells were pre-treated with Anti-miR-21 nanoplexes for 48 h. Following the treatment, the media were aspirated and replaced by a medium containing 5 or 10 μM cis-Pt. After 24 h MTT assay was performed according to the aforementioned method.

2.8. *Live/Dead assay*

In order to discriminate live, apoptotic and necrotic cells under fluorescent microscope, Acridine Orange (AO)/ Ethidium Bromide (EtBr) double-staining assay was performed. 7×10^5 cells/well of A2780S and A2780R cells were seeded in 24-well plates, treated with the nanoplexes (N/P = 5) for 72 h. Then, the cells were trypsinized, stained with AO/EtBr dye mix in PBS (100 μg/ml) and observed under fluorescent microscope (Nikon Eclipse E400, Japan) [46].

2.9. *Statistics*

Statistical analysis was performed using Prism Software version 5.0 (GraphPad, USA). P values less than 0.05 were considered statistically significant. Data were expressed as mean ± standard deviation.

3. Results and discussion

3.1. *Physicochemical characterization of the nanogels*

In present study to investigate the effects of structural variation of PEG2k-PEI copolymer on transfection of Anti-miR-21, synthesis of PEG2k-PEI-ss nanogels containing redox-sensitive crosslinks [33] and the carboxymethylated nanogels (PEG2k-CMPEI-ss) have been done. Synthesis of PEG2k-PEI copolymer and the PEG2k-PEI-ss nanogels were confirmed by ^{1}H NMR, FTIR and DLS methods as reported previously [33]. Following the carboxymethylation reaction, TNBS assay was used in order to monitor changes in the concentration of primary amine residues [47,48], considering that the reactions involves often the PEI primary amines [49]. Using the calibration curve plotted for standard glycine solutions, it was found that about 14.7% of the PEG2k-PEI primary amines were consumed to produce simple nanogels and 87.0% of the remaining amines were used to produce PEG2k-CMPEI-ss nanogels, so less than 10% of the available primary amines were only present in chemical structure of the resulting nanogels, but still sufficient for the fluorescent labeling of nanogels [50].

Following the carboxymethylation reaction, the chemical structure of nanogels were investigated by FTIR and ^{1}H NMR spectroscopy. The peaks at 3420, 1113 and 1669 cm^{-1} is attributed to N–H, C–O and amide C=O stretching of PEI, PEG2k and the crosslinker DTDP in the PEG2k-PEI-ss nanogels, respectively. After carboxymethylation reaction, the unique

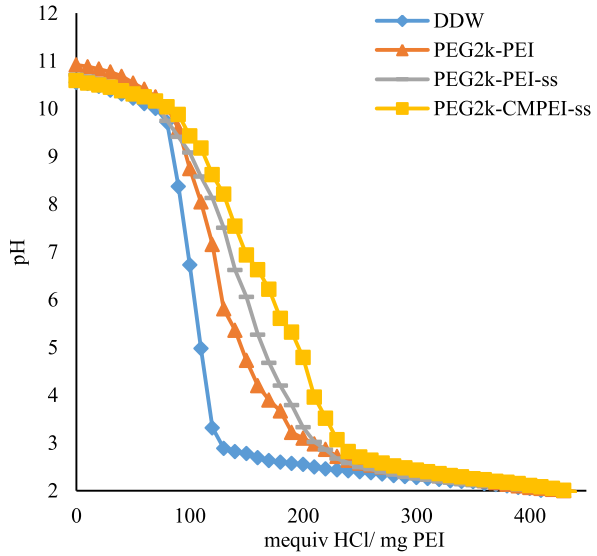

Fig. 1 – Back-titration curve of PEG2k-PEI copolymer, PEG2k-PEI-ss and PEG2k-CMPEI-ss nanogels at a quantity corresponding to 1 mg PEI after supplementing the medium (double distilled water, DDW) with 20 μl of 1 N NaOH.

broad peak at 2500—3000 cm^{-1} appears that is related to the hydroxyl group of carboxylic acid moieties (suplementary data) as reported before [51]. The degree of carboxymethylation was determined by ^{1}H NMR. The peaks at 3.4 and 2.3–3.3 ppm are related to CH_2–O of PEG and CH_2–N of PEI in the spectrum of the PEG2k-PEI-ss nanogel. The specific peak of CH_2–CH_2–COOH in the PEG2k-CMPEI-ss nanogel structure is also located at 2.3–3.3 ppm, so the area under the curve of this range increased (suplementary data). Degree of carboxymethylation was estimated about 44% for total primary and secondary amines.

Potentiometric titration was performed to determine the variation in buffer capacity of PEG2k-PEI copolymer following synthesis of the nanogels at the concentration corresponding to 3.3 mg/ml PEI (Fig. 1). It was revealed that the titration curves shifted to the right following the crosslinking reaction (PEG2k-PEI-ss). A further shift in acidic pH occurred after carboxymethylation reaction that is responsible not only for increasing the buffering capacity and endosomal escape properties, but also for reducing the cytotoxicity induced by the positively charged nanoparticles [51]. The maximum buffer capacity was determined in pH 5.3 corresponding to pKa of the carboxylic acid groups that exist in the core of PEG2k-CMPEI-ss nanogels [52].

Ellman's assay method was done for determination of free thiols recovered after treating the nanogels with a reducing agent ($NaBH_4$). Unlike untreated polymers, the free thiol concentrations were determined 0.14 ± 0.02 and 0.10 ± 0.01 mM for PEG2k-PEI-ss and PEG2k-CMPEI-ss nanogels, respectively. The concentrations of recovered free thiols were consistent with estimated density of the crosslinks.

3.2. *Biological characterization of the nanoplexes*

Gel retardation assay was carried out to investigate the nanoplex formation after adding Anti-miR-21 to PEG2k-PEI,

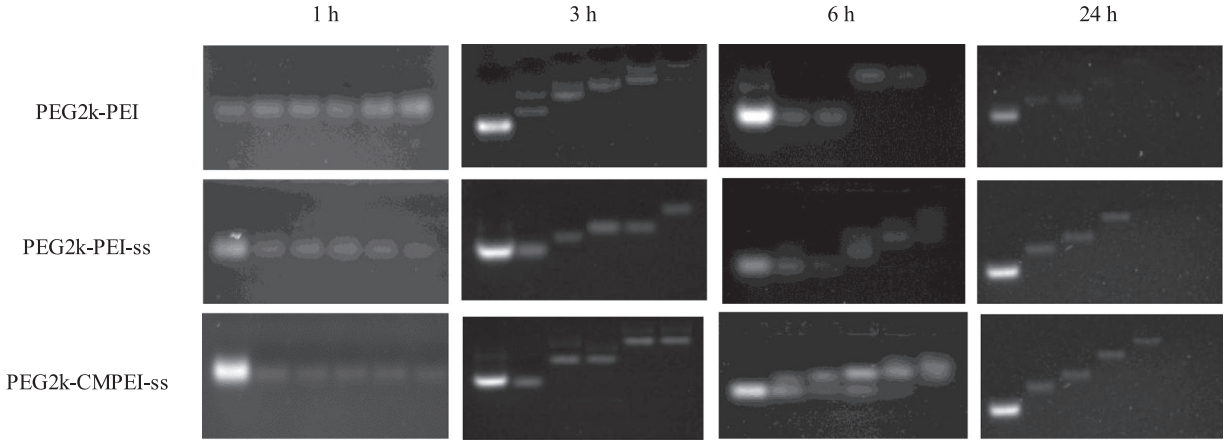

Fig. 2 – Gel retardation assay at various incubation times and N/P ratios (lanes from left to right: 0, 0.5, 1, 2, 5, 10).

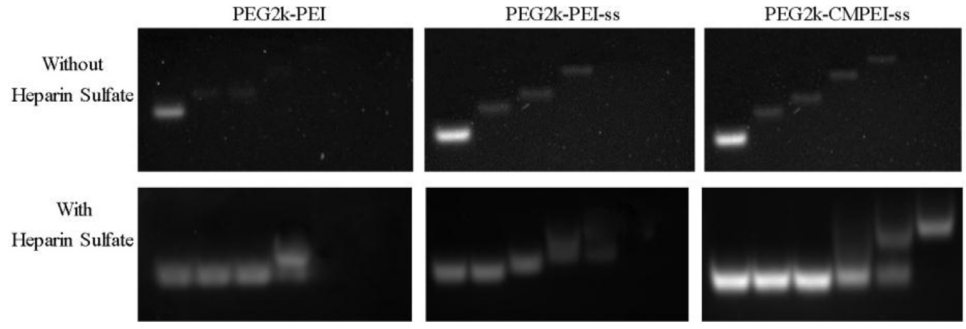

Fig. 3 – Retardation of Anti-miR-21 loaded in the nanoplexes at various N/P ratios (lanes from left to right: 0, 0.5, 1, 2, 5, 10) with or without adding heparin sulfate.

PEG2k-PEI-ss or PEG2k-CMPEI-ss nanogels using agarose gel electrophoresis [53]. Retardation of the oligonucleotide band was noticed by increasing N/P ratios and the incubation time until no residual naked oligonucleotide band was seen in the gel as reported by others [54]. Depending on the chemical nature and structure of the polymers, the optimum N/P molar ratio was different [55]. In our experiment, at low N/P ratios of 0.5–1, the cationic charge was insufficient to neutralize and condense the negatively charged Anti-miR-21 even after long incubation times as reported elsewhere [54]. However, upon increasing N/P ratios as well as the incubation time, the migration of Anti-miR-21 was retarded in the gel so that no migration happens in the gel for N/P as low as 5 and a prolonged incubation time of 3–24 h, indicating a complete neutralization of Anti-miR-21 negative charge through a complete nanoplex formation (Fig. 2). The nanoplexes formed almost completely with PEG2k-PEI copolymer and PEG2k-PEI-ss nanogels similarly at N/P ratio as low as 2, but the required incubation times were different (3 h *vs.* 24 h for the uncrosslinked copolymer and the nanogel, respectively) (Fig. 2). The N/P ratio shifted to the higher value of 5 for PEG2k-CMPEI-ss nanogels. A relatively prolonged incubation time is required for Anti-miR-21 loading into the nanogels possibly due to crosslinks in the polycation network that can hinder DNA penetration for subsequent complex formation as reported by Hartlieb et al. [56].

Biologic stability of nanoplexes is a pre-requisite for successful transfection. It has been reported that biologic stability of nanoplexes is related to polymer structure and N/P ratio [50]. So, the nanoplexes were exposed to heparin sulfate for determination of possible nucleic acid displacement [57]. In this issue, the nanoplex structure can be disrupted and Anti-miR-21 may be released following exposure to the extracellular matrix due to the polyanionic nature of heparin sulfate [58]. As shown in Fig. 3, unlike the PEG2k-CMPEI-ss nanogels that resist against heparin sulfate-induced displacement of oligonucleotides at N/P ratio = 10, no displaced oligonucleotide band was seen at N/P ratio as low as 5 similarly for the uncrosslinked PEG2k-PEI and PEG2k-PEI-ss nanogels, indicating a complete protection against extracellular matrix. So, the results suggest that the crosslinking reaction provides convenient networks to capture Anti-miR-21 and lessen displacement induced by heparin sulfate. Although there are generally more accessible cationic amines in the uncrosslinked polycation (PEG2k-PEI) than the nanogels (PEG2k-PEI-ss and PEG2k-CMPEI-ss) to condense and neutralize negative charges of Anti-miR-21, the instability is less prominent for PEG2k-PEI-ss nanogel possibly due to adequacy of the network structure to prevent heparin sulfate interaction.

EtBr dye exclusion assay was also carried out in order to analysis of the nanoplex formation and the resistance against heparin sulfate [59]. Intercalation of the EtBr with

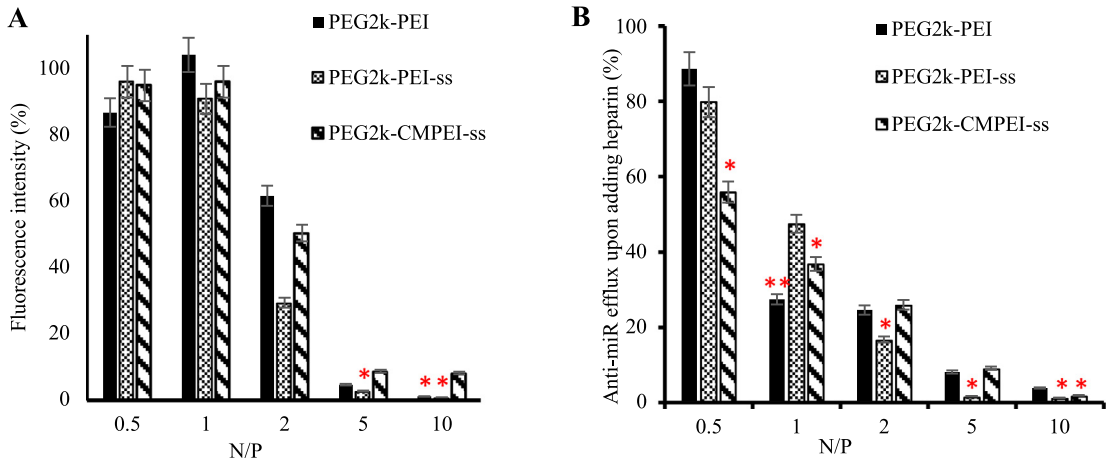

Fig. 4 – (A) EtBr dye exclusion assay. (B). Polyanion competition assays after adding heparin sulfate. *, symbols represent statistically significant differences between treatments for each N/P ratio: *$P < 0.05$, **$P < 0.01$.**

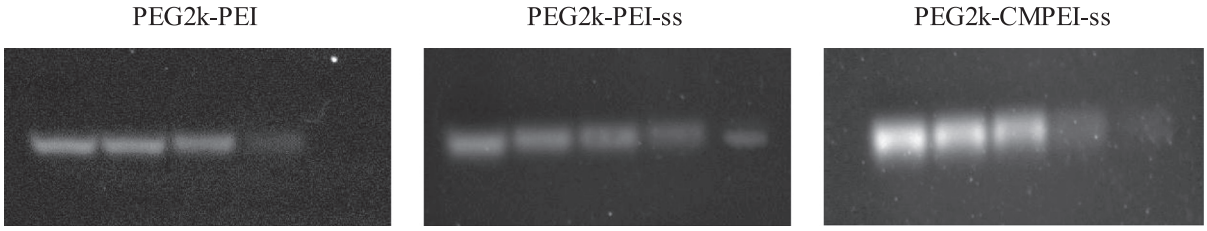

Fig. 5 – DNase I digestion assay in agarose gel at various incubation times; lanes from left to right: 0, 1, 3, 6, 24 h.

oligonucleotides results in fluorescence intensity enhancement which decreases upon adding polycations as a result of the fluorescent probe exclusion from their intercalation sites [57,60,61]. The fluorescence intensity of intercalated EtBr was determined at different N/P ratios. As shown in Fig. 4A, by increasing the N/P ratios, the fluorescence intensity decreased, indicating oligonucleotide sequestration by the polycations. However, PEG2k-PEI-ss nanogel was the most efficient polymer in capturing Anti-miR-21 oligonucleotide, the difference was more recognized at N/P = 2. For further characterization of the nanoplexes, polyanion (heparin sulfate) competition assay was performed. Fig. 4B shows that heparin sulfate triggered the release of Anti-miR-21 oligonucleotide from the nanoplexes. PEG2k-PEI-ss nanogels show a better condensation of Anti-miR-21 than uncrosslinked PEG2k-PEI and less efflux of the loaded Anti-miR-21 following heparin sulfate treatment. It was believed that introduction of carboxylate negative charge through carboxymethylation of the nanogels (PEG2k-CMPEI-ss) may decrease competitive binding of the nanogels to condense and protect Anti-miR-21. Therefore at a sufficient nanogel concentration (N/P = 5), no practically significant efflux of the oligonucleotide was seen.

3.3. *Stability of nanoplexes against DNase I*

DNase I digestion assay was done to evaluate Anti-miR-21 protection provided by the polycations against nucleases at N/P of 5. Fig. 5 shows that although all polycations can protect the oligonucleotide against enzymatic degradation, PEG2k-PEI-ss and PEG2k-CMPEI-ss nanogels were more efficient than uncrosslinked PEG2k-PEI copolymer in protecting Anti-miR-21 after prolonged incubation times. This might be as the result of slow penetration of high molecular weight nucleases into the PEGylated nanogel network provided by crosslinking reactions [62].

3.4. *Particle size and ζ potential*

Colloidal properties (particle size and ζ potential) of the nanogels and the resulting nanoplexes are among the factors that determines stability, transfection activity and biocompatibility. Particle size and ζ potential values were determined before and after loading Anti-miR-21 at N/P = 5.

As presented in Table 1, ζ potentials of the nanogels are inversely correlated with the protonable amine density. Although less aggregation may occur for the higher ζ zeta-potentials due to greater electrostatic repulsion, no colloidal instability was determined for PEG2k-CMPEI-ss. Moreover, the particle sizes was determined less than those of PEG2k-PEI-ss possibly due to salt bridges between amines and carboxylate moieties resided within the nanogel structure. Following polyplex formations, reduction of the sizes and ζ potentials probably arises from the formation of tight complexes with Anti-miR-21 [63] that were determined identical for the uncrosslinked copolymer and the nanogels at N/P ratio of 5. Although the mechanism by which oligonulcoetide interacts with PEG2k-PEI may differ from the crosslinked structures, no

Table 1 – Z-average, polydispersity index (PDI) and ζ potential (mean ± SD) of the polycations alone and after loading with Anti-miR-21 at N/P = 5.

Polycation	Z-average (nm)		PDI		ζ potential (mV)	
	Alone	+ Anti-miR-21	Alone	+ Anti-miR-21	Alone	+ Anti-miR-21
PEG2k-PEI	ND*	270	ND*	0.23	+ 27.3 ± 0.83	− 20.23 ± 0.61
PEG2k-PEI-ss	366	289	0.31	0.35	+ 18.3 ± 2.28	− 30.97 ± 1.95
PEG2k-CMPEI-ss	234	234	0.60	0.57	+ 12.2 ± 0.99	− 34.27 ± 2.05

* Not determined.

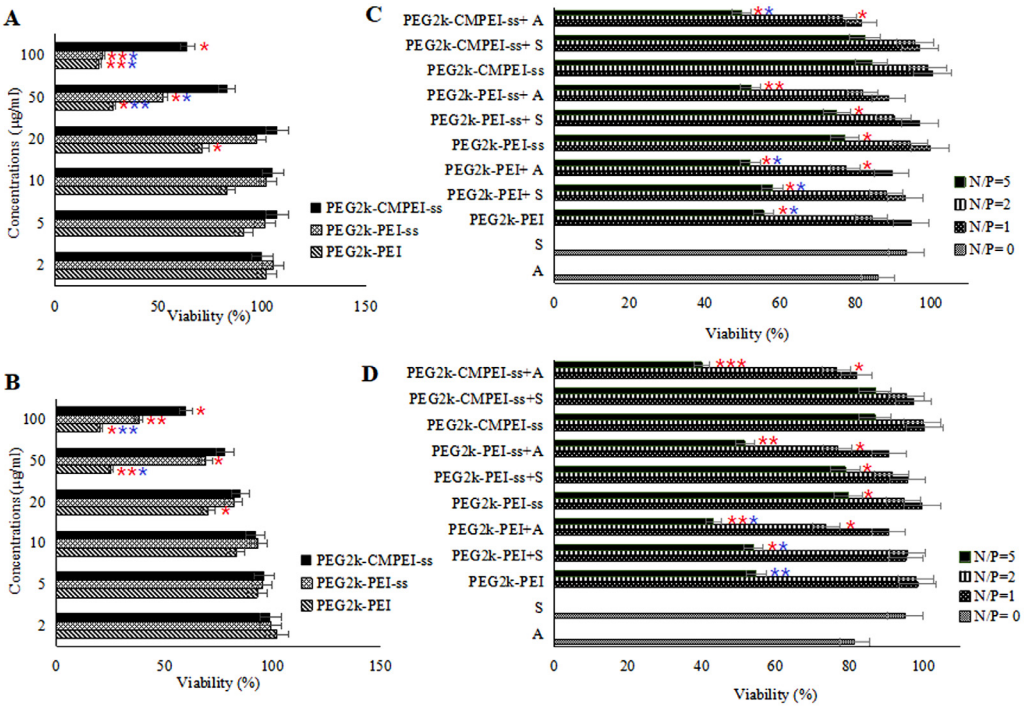

Fig. 6 – MTT-based cytotoxicity of PEG2k-PEI, PEG2k-PEI-ss and PEG2k-CMPEI-ss nanogels alone in A2780S (A) and A2780R (B) cell lines at various concentrations. (C) and (D) the respective viability of A2780S and A2780R cells following treatment with the Anti-miR-21 nanoplexes prepared at various N/P mole ratios for 72 h. The symbols denote statistically significant differences from the least cytotoxic treatment: *P < 0.05, **P < 0.01 and ***P < 0.0001.

significant effect was found on the size and ζ potential possibly due to presence of the stabilizing PEG shell.

3.5. Cytotoxicity

3.5.1. MTT assay

Cytotoxicity of polycations is almost a challengeable factor for successful gene delivery [64]. To investigate first the cytocompatibility of nanogels, the cell viability was determined by (a) MTT assay of the intracellular metabolic activity and (b) trypan blue exclusion assay that depends on the integrity of the cellular membrane. Then, the sequence-specific cell growth inhibition induced by the Anti-miR-21 loaded nanogels was investigated as a function of N/P mole ratios (N/P = 1, 2 and 5) in A2780S and A2780R cell lines. As shown in Fig. 6A and 6B, neither PEG2k-PEI copolymer nor the nanogels showed any significant cytotoxicity at concentrations as low as 10 μg/ml ($P < 0.05$). However, their cytotoxicity increased by the polymer concentration so that the cell viability decreased significantly at 50 and 100 μg/ml in both A2780S ($P < 0.0001$) and A2780R ($P < 0.01$) cells. In addition, it was revealed that the cytotoxicity of PEG2k-CMPEI-ss nanogels at the concentration of 100 μg/ml was significantly lower than PEG2k-PEI-ss nanogels in A2780S and A2780R ($P < 0.0001$). The cytotoxicity results can be explained according to primary amine contents of the polycations [51,65] which cause interactions with negatively charged molecules located on the cell surface [64]. It has been shown that crosslinking of PEG2k-PEI reduces cell toxicity significantly due to core-shell structure of the nanogels that provides a better PEG shielding [33]. On the other hand, carboxymethylation of the nanogels further improves the cell compatibility which may be due to reduced pK_a of PEG2k-PEI and higher buffer capacity of PEG2k-CMPEI-ss in acidic pH as demonstrated in Fig. 1. The lower pK_a leads to reduced protonation of the nanogels and the lower positive ζ potentials at physiologic pH (Table 1) that lessons the cell toxicity [51,66].

Table 2 – Trypan blue assay of the cell membrane leakage induced by the polymers either alone or in combination with Anti-miR-21 (N/P = 5).

Polycation	Condition	Membrane leakage (%)	
		A2780S	A2780R
PEG2k-PEI	alone	21.9 ± 7.6*	19.7 ± 4.0
	+ Anti-miR-21	26.9 ± 3.6*	25.5 ± 5.3*
PEG2k-PEI-ss	alone	14.3 ± 4.7	17.6 ± 3.1
	+ Anti-miR-21	36.8 ± 6.1*	43.9 ± 3.4**
PEG2k-CMPEI-ss	alone	12.2 ± 4.7	13.1 ± 3.6
	+ Anti-miR-21	50.0 ± 1.8***	54.2 ± 2.7***

Symbols denotes significant differences within each column: *$P < 0.05$, **$P < 0.01$, ***$P < 0.001$.

Fig. 6C and D shows that Anti-miR-21 loaded nanogels applied significant effects on the cells viability in comparison to either naked Anti-miR-21 or the empty nanogels. Indeed, it was found that the nanoplexes did not show practically significant cytotoxicity at N/P = 1 and 2, however at N/P = 5, A2780R was more sensitive in response to the Anti-miR-21 treatment than A2780S ($P < 0.05$). Treatment of A2780S cells with PEG2k-PEI, PEG2k-PEI-ss and PEG2k-CMPEI-ss nanogels loaded with Anti-miR-21 at N/P = 5 led to cell viability decrement (if compared to unloaded nanoparticles) by 4% ($P < 0.05$), 24% ($P < 0.0001$) and 35% ($P < 0.0001$), respectively; while the decrements were determined more in A2780R cell lines, 11% ($P < 0.01$), 28% ($P < 0.0001$) and 47% ($P < 0.0001$), respectively. The nanogels loaded with the scrambled sequence did not show any significant effect on the cell viability. Treating A2780S cells with PEG2k-PEI, PEG2k-PEI-ss and PEG2k-CMPEI-ss nanogels loaded with Anti-miR-21 at N/P = 5 led to cell viability decrement while the decrements were determined more in A2780R cell lines which can be explained by the abbarent expression of miR-21 in A2780R compared to A2780S cell lines.

3.5.2. *Cell membrane leakage assay*

Trypan blue membrane leakage assay was done in order to examine whether the nanogels either alone or after loading with Anti-miR-21 at N/P = 5 brought about toxic effects on A2780 cell lines that led to the cell membrane leakage and the cell death. Table 2 shows the cell viability changes when incubated with the nanogels for a prolonged period of 24 h. Unlike the nanogel treatment alone that showed a modest toxicity, the Anti-miR-21 nanoplexes prepared at the corresponding nanogel concentration (N/P = 5) produced significant toxicity ($P < 0.05$). The effect was more pronounced for PEG2k-CMPEI-ss nanogels similarly in A2780S and A2780R cells that may be due to efficient delivery of Anti-miR-21 causing loss of cell membrane integrity [67].

3.6. *Cellular uptake and intracellular release*

Following nanoplex formation, the oligonucleotide charge neutralization and condensation happens that can promote oligonucleotide interaction with the negatively charged cell membrane and cause cellular internalization especially at high N/P ratios [68,69]. The cellular uptake of nanoplexes is mainly energy dependent through different mechanisms such as clathrin-mediated endocytosis [38]. After having incubated the cells for 1 h with FITC-labeled polycations, the fluorescence microscopy experiment was performed that shows green fluorescence in cytoplasm due to cellular binding and endosomal uptake in A2780 cell lines (Fig. 7A). The fluorescence was more intense in A2780R than A2780S cells. Cytoplasmic localization of the polycations was found after staining the nuclei by DAPI (blue color) to make the required contrast. The green dotted pattern was noticed in the proximity of cell membranes for the polycations having co-treated the cells with dextran-FITC. More uniform green fluorescence was observed 4 h after treating the cells, indicating endosomal release into cytoplasm (Fig. 7B). The release was more around the cell nuclei for PEG2k-CMPEI-ss in comparison to PEG2k-PEI and PEG2k-PEI-ss nanogel. Carboxymethylation of PEG2k-PEI nanogels lowers pka and increases buffer capacity of the nanogels in more acidic pH of late endosomes (Fig. 1); therefore, the endosomal escape can occur more effectively far from the cell membrane and more close to the nucleus possibly through well-known proton sponge mechanism [27]. To further investigate the endosomal release, co-localization experiment of the FITC labeled nanogel with Lysotracker is suggested.

3.7. *miR-21 expression*

Cellular uptake and endosomal release of Anti-miR-21 can result in miR-21 knockdown as reported elsewhere [70]. Relative expression levels of miR-21 after treating A2780S and A2780R cell lines with Anti-miR-21 and the scrambled sequence, either naked or loaded in the nanogels, are shown in Fig. 8A. The results clearly demonstrate that the loaded Anti-miR-21 downregulated miR-21 expression whereas the loaded scrambled sequence or the naked Anti-miR-21 did not show any significant effects as reported elsewhere [71]. This result indicates the gene knockdown is sequence-specific and needs neutralization of the negative charge of Anti-miR-21 for a successful transfection [71]. The efficiency of gene silencing was absolutely more remarkable in A2780R than A2780R cells. Moreover, the downregulation of miR-21 was more evident in the cell lines treated with Anti-miR-21 loaded in PEG2k-CMPEI-ss nanogels. No changes in ß-actin expression (the housekeeping gene as shown in Fig. 8B) was detected. As reported in literature, the positive charges enhance cells interactions, cellular uptake and endosomal release [70] that might result in miR-21 knockdown. On the other hand, enhanced endosomal release as presented in Fig. 7B might have significant effects in cytoplasmic release of Anti-miR-21 and consequently microRNA-21 down-regulation.

3.8. *Effect of miR-21 downregulation on cis-Pt resistance*

It has been revealed that miR-21 overexpression is directly related to drug resistance [17,20,72–75]. cis-Pt treatment alone did not exert any significant cytotoxicity either in A2780S or A2780R in the concentrations below 20 µM (Fig. 9A). As shown in Fig. 9B, treating cells with cis-Pt after 48 h incubation with Anti-miR-21 loaded nanogels sensitized cells remarkably to cis-Pt, even in its low concentrations

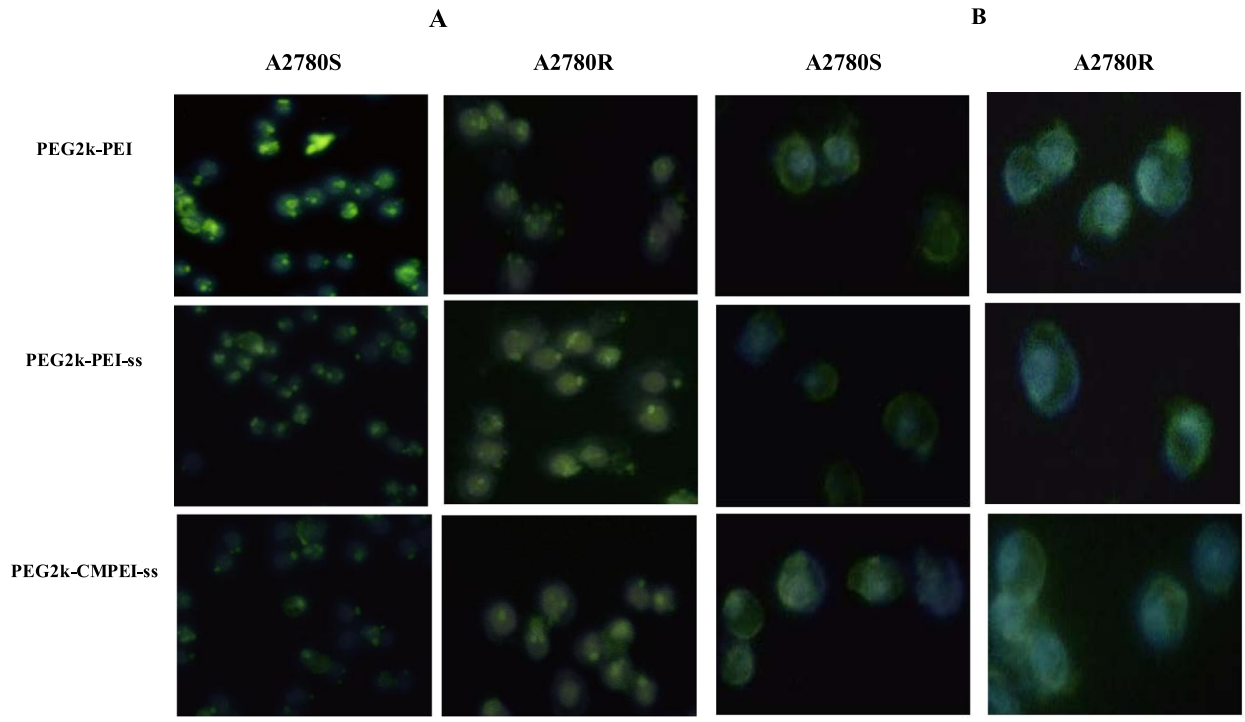

Fig. 7 – Images of the internalized FITC-labeled polymers in A2780R and A2780S cell lines: cellular uptake after 1 h incubation (A) and endosomal release of FITC-dextran co-treated with the polymers after 4 h incubation (B) at 37 °C (all figures were overlaid with DAPI stained cell nuclei).

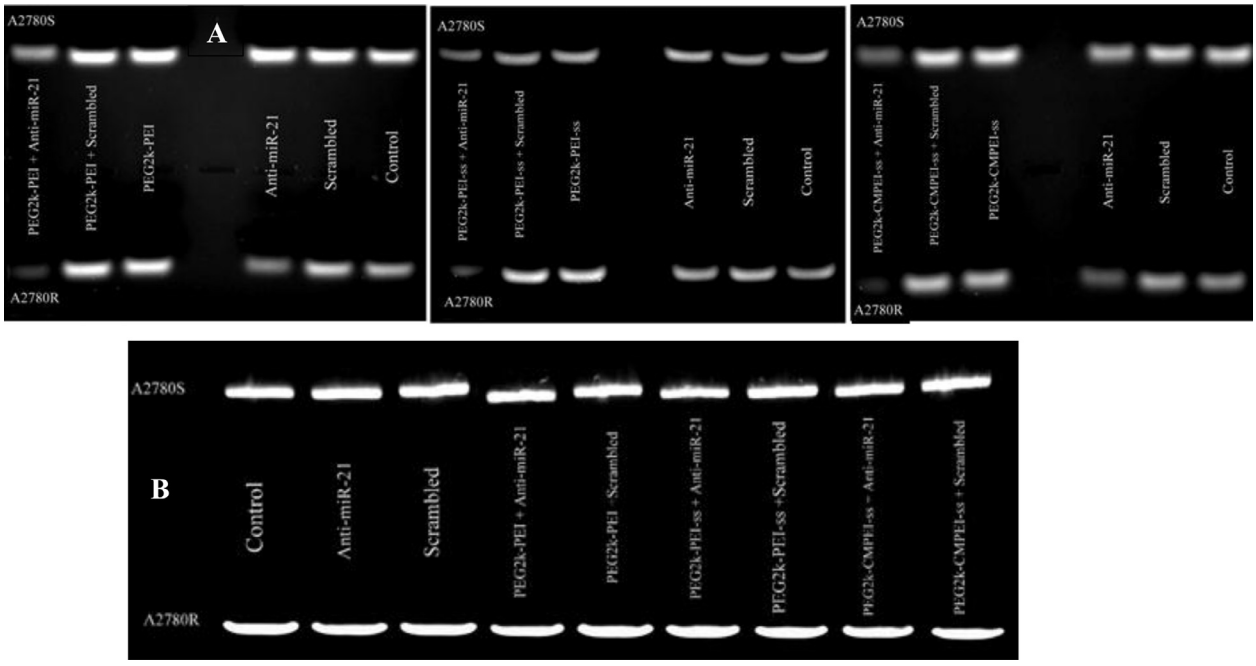

Fig. 8 – (A) Expression of miR-21 in A2780S and A2780R cell lines 72 h after treatment with Anti-miR-21 (A) or the scrambled sequence (S) either naked or the nanoplexes prepared with PEG2k-PEI copolymer, PEG2k-PEI-ss and PEG2k-CMPEI-ss nanogels. (B) Expression of ß actin.

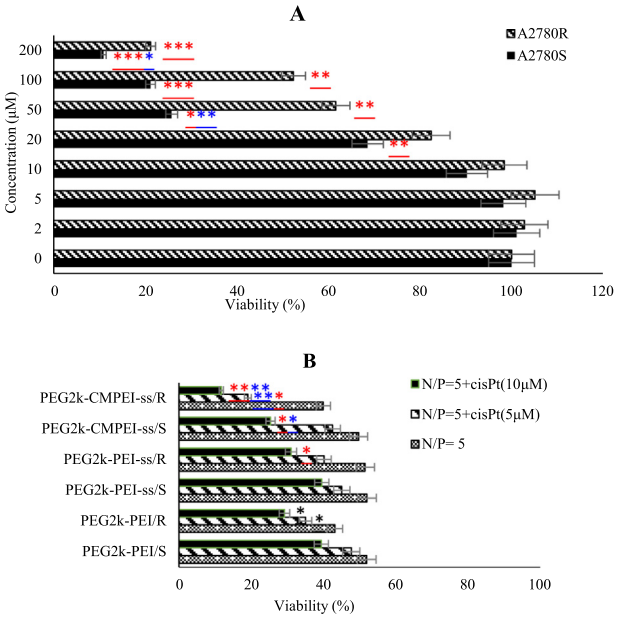

Fig. 9 – (A) Viability of A2780S and A2780R cell lines after treatment with cis-Pt in the range of 2–200 μM. (B) Viability of the cells pre-treated with Anti-miR-21 loaded nanogels (N/P = 5) and after treatment with cis-Pt. Abbreviations: R and S represent A2780R and A2780S cells, respectively. The symbols denote statistically significant differences from the least cytotoxic treatment: * $P < 0.05$, ** $P < 0.01$, *** $P < 0.001$ and **** $P < 0.0001$.

(5 and 10 μM). This observation can be explained by the research finding that down-regulation of miR-21 could sensitize A2780R to cis-Pt through down-regulation of PTEN expression and JNK-1/c-Jun/miR-21 pathway [18]. Indeed, it has been revealed that A2780R is more sensitive in response to Anti-miR-21 treatment than A2780S at N/P = 5 that may be due to the aberrant miR-21 expression in A2780R compared to A2780S (Fig. 9B) [18].

3.9. *Live / dead assay*

As demonstrated in Fig. 10, live cells with normal morphology can be observed in the untreated control or the scrambled sequence loaded nanogels. On the other hand, early and late apoptotic cells were recognized in the cells treated with Anti-miR-21 loaded PEG2k-CMPEI-ss nanogels (42% ± 6.4% and 56% ± 1.6% of live cells in A2780R and A2780S, respectively). Thus, cellular DNA damage mediated by apoptosis and secondary necrosis, was remarkably induced after Anti-miR-21 loaded PEG2k-CMPEI-ss nanogels treatment (Fig. 10), probably because of enhanced endosomal release of Anti-miR-21 as presented in Fig. 7B, which can potentiate the expression of tumor suppressor PDCD4 and revoked apoptosis inhibitor c-IAP2 [22].

4. Conclusion

Various PEI modifications including PEG2k-PEI copolymer, PEG2k-PEI-ss and PEG2k-CMPEI-ss nanogels have been prepared to improve transfection of Anti-miR-21. Although the

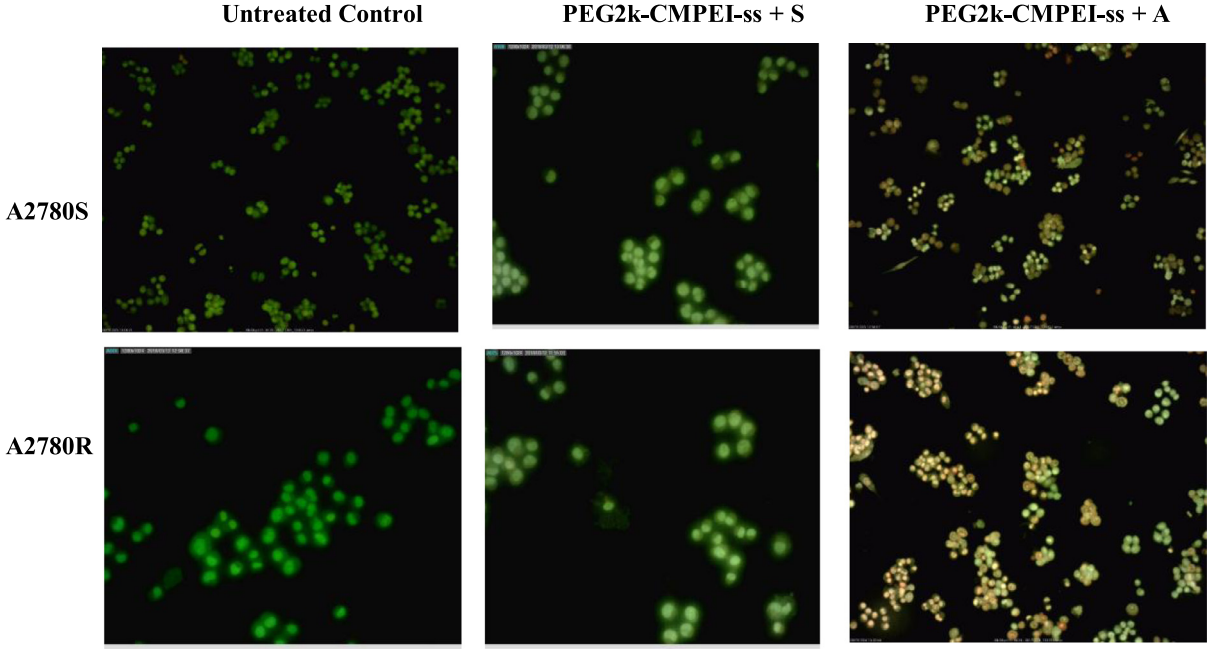

Fig. 10 – Fluorescence microscopy images of the cells treated with Anti-miR-21 and Scrambeled sequence loaded nanogels *vs.* untreated control cells. Green live cells showed normal morphology; yellowish-green early apoptotic cells showed nuclear margination and chromatin condensation, while late orange apoptotic cells showed fragmented chromatin and apoptotic bodies.

cross-linking and carboxymethylation reactions decrease primary amine contents of the PEG2k-PEI needed for oligonucleotide charge neutralization and condensation, protonation of primary amines at physiologic pH and the general cytotoxicity are diminished. Moreover, the nanogels can effectively protect Anti-miR-21 against extracellular matrix and also DNase digestion. Notably, an enhanced endosomal escape and transfection efficiency are determined for the nanogels. Therefore, PEG2k-CMPEI-ss nanogels is proposed as a potential nano-vector for Anti-miR-21 delivery and a basis for future dual delivery with chemotherapeutic agents. Investigation of cellular trafficking of the nanogels, the biologic consequences of miR-21 down-regulation and molecular mechanisms of cis-Pt chemosensitization by the nanoplexes are suggested for further study.

Compliance with ethical standards

Conflicts of interest: The authors declare that they have no conflict of interest.

Acknowledgment

This work was supported financially by Shiraz University of Medical Sciences (Grant No: SUMS-93-01-05-8630). The facility supports of "Center for Nanotechnology in Drug Delivery" are gratefully acknowledged.

Supplementary materials

Supplementary material associated with this article can be found, in the online version, at doi:10.1016/j.ajps.2018.10.006.

REFERENCES

[1] Baru L, Patnaik R, Singh KB. Clinico pathological study of ovarian neoplasms. IJRCOG 2017;6:3438–44.
[2] Hunn J, Rodriguez GC. Ovarian cancer: etiology, risk factors, and epidemiology. Clin Obstet Gynecol 2012;55:3–23.
[3] Hempling RE, Wong C, Piver MS, Natarajan N, Mettlin CJ. Hormone replacement therapy as a risk factor for epithelial ovarian cancer: results of a case-control study. Obstet Gynecol 1997;89:1012–16.
[4] Ries LAG. Ovarian cancer: survival and treatment differences by age. Cancer 1993;71:524–9.
[5] Andrews PA, Velury S, Mann SC, Howell SB. cis-Diamminedichloroplatinum (II) accumulation in sensitive and resistant human ovarian carcinoma cells. Cancer Res 1988;48:68–73.
[6] Ikeguchi M, Nakamura S, Kaibara N. Quantitative analysis of expression levels of bax, bcl-2, and survivin in cancer cells during cisplatin treatment. Oncol Rep 2002;9:1121–6.
[7] Ganesh S, Iyer AK, Weiler J, Morrissey DV, Amiji MM. Combination of siRNA-directed gene silencing with cisplatin reverses drug resistance in human non-small cell lung cancer. Mol Ther Nucleic Acids 2013;2:e110.
[8] Pillai RS. MicroRNA function: multiple mechanisms for a tiny RNA? RNA 2005;11:1753–61.
[9] Lee RC, Feinbaum RL, Ambros V. The C. elegans heterochronic gene lin-4 encodes small RNAs with antisense complementarity to lin-14. Cell 1993;75:843–54.
[10] Dai R, Ahmed SA. MicroRNA, a new paradigm for understanding immunoregulation, inflammation, and autoimmune diseases. Transl Res 2011;157:163–79.
[11] Sekar D, Venugopal B, Sekar P, Ramalingam K. Role of microRNA 21 in diabetes and associated/related diseases. Gene 2016;582:14–18.
[12] Saghazadeh A, Rezaei N. MicroRNA machinery in Parkinson's disease: a platform for neurodegenerative diseases. Expert Rev Neurother 2015;15:1–27.
[13] Ge Y, Chen G, Sun L, Liu F. MicroRNA-29 and fibrosis diseases. Zhong Nan Da Xue Xue Bao Yi Xue Ban 2011;36:908–12.
[14] Cao RY, Li Q, Miao Y, Zhang Y, Yuan W, Fan L, et al. The emerging role of microRNA-155 in cardiovascular diseases. Biomed Res Int 2016;2016:1–5.
[15] Calin GA, Croce CM. MicroRNA-cancer connection: the beginning of a new tale. Cancer Res 2006;66:7390–4.
[16] Javanmardi S, Reza Aghamaali M, Sadat Abolmaali S, Mohammadi S, Mohammad Tamaddon A. miR-21, an oncogenic target miRNA for cancer therapy: molecular mechanisms and recent advancements in chemo and radio-resistance. Curr Gene Ther 2016;16:375–89.
[17] Chan JK, Blansit K, Kiet T, Sherman A, Wong G, Earle C, et al. The inhibition of miR-21 promotes apoptosis and chemosensitivity in ovarian cancer. Gynecol Oncol 2014;132:739–44.
[18] Echevarría-Vargas IM, Valiyeva F, Vivas-Mejía PE. Upregulation of miR-21 in cisplatin resistant ovarian cancer via JNK-1/c-Jun pathway. PLoS One 2014;9:e97094.
[19] Liu S, Fang Y, Shen H, Xu W, Li H. Berberine sensitizes ovarian cancer cells to cisplatin through miR-21/PDCD4 axis. Acta Biochim Biophys Sin 2013;45:756–62.
[20] Xie Z, Cao L, Zhang J. miR-21 modulates paclitaxel sensitivity and hypoxia-inducible factor-1α expression in human ovarian cancer cells. Oncol Lett 2013;6:795–800.
[21] Li J, Jiang K, Zhao F. Icariin regulates the proliferation and apoptosis of human ovarian cancer cells through microRNA-21 by targeting PTEN, RECK and Bcl-2. Oncol Rep 2015;33:2829–36.
[22] Chan JK, Blansit K, Kiet T, Sherman A, Wong G, Earle C, et al. The inhibition of miR-21 promotes apoptosis and chemosensitivity in ovarian cancer. Gynecol Oncol 2014;132:739–44.
[23] Aied A, Greiser U, Pandit A, Wang W. Polymer gene delivery: overcoming the obstacles. Drug Discov Today 2013;18:1090–8.
[24] Lollo CP, Banaszczyk MG, Chiou HC. Obstacles and advances in non-viral gene delivery. Curr Opin Mol Ther 2000;2:136–42.
[25] Baker A, Saltik M, Lehrmann H, et al. Polyethylenimine (PEI) is a simple, inexpensive and effective reagent for condensing and linking plasmid DNA to adenovirus for gene delivery. Gene Ther 1997;4:773–82.
[26] Meneksedag-Erol D, Tang T, Uludağ H. Probing the effect of miRNA on siRNA–PEI polyplexes. J Phys Chem B 2015;119:5475–86.
[27] Benjaminsen RV, Mattebjerg MA, Henriksen JR, Moghimi SM, Andresen TL. The possible "proton sponge" effect of polyethylenimine (PEI) does not include change in lysosomal pH. Mol Ther 2013;21:149–57.
[28] Søndergaard RV, Mattebjerg MA, Henriksen JR, Moghimi SM, Andresen TL. The possible" proton sponge" effect of polyethylenimine (PEI) does not include change in lysosomal pH. Mol Ther 2013;21:149–57.
[29] Thomas M, Klibanov AM. Enhancing polyethylenimine's delivery of plasmid DNA into mammalian cells. PNAS 2002;99:14640–5.

[30] Oskuee RK, Philipp A, Dehshahri A, Wagner E, Ramezani M. The impact of carboxyalkylation of branched polyethylenimine on effectiveness in small interfering RNA delivery. J Gene Med 2010;12:729–38.
[31] Sakae M, Ito T, Yoshihara C, Iida-Tanaka N, Yanagie H, Eriguchi M, et al. Highly efficient *in vivo* gene transfection by plasmid/PEI complexes coated by anionic PEG derivatives bearing carboxyl groups and RGD peptide. Biomed Pharmacother 2008;62:448–53.
[32] Hoffmann C, Stuparu MC, Daugaard A, Khan A. Aza-Michael addition reaction: Post-polymerization modification and preparation of PEI/PEG-based polyester hydrogels from enzymatically synthesized reactive polymers. J Polym Sci A Polym Chem 2015;53:745–9.
[33] Abolmaali SS, Tamaddon AM, Dinarvand R. Nano-hydrogels of methoxy polyethylene glycol-grafted branched polyethyleneimine via biodegradable cross-linking of Zn^{2+}-ionomer micelle template. J Nanopart Res 2013;15:2134.
[34] Najafi H, Abolmaali SS, Owrangi B, Ghasemi Y, Tamaddon AM. Serum resistant and enhanced transfection of plasmid DNA by PEG-stabilized polyplex nanoparticles of L-histidine substituted polyethyleneimine. Macromol Res 2015;23:618–27.
[35] Raemdonck K, Demeester J, De Smedt S. Advanced nanogel engineering for drug delivery. Soft Matter 2009;5:707–15.
[36] Dunn SS, Tian S, Blake S, et al. Reductively responsive siRNA-conjugated hydrogel nanoparticles for gene silencing. JACS 2012;134:7423–30.
[37] Creusat G, Rinaldi AS, Weiss E, Elbaghdadi R, Remy JS, Mulherkar R, et al. Proton sponge trick for pH-sensitive disassembly of polyethylenimine-based siRNA delivery systems. Bioconjug Chem 2010;21:994–1002.
[38] Abolmaali SS, Tamaddon AM, Mohammadi S, Amoozgar Z, Dinarvand R. Chemically crosslinked nanogels of PEGylated poly ethyleneimine (l-histidine substituted) synthesized via metal ion coordinated self-assembly for delivery of methotrexate: cytocompatibility, cellular delivery and antitumor activity in resistant cells. Mater Sci Eng C Mater Biol Appl 2016;62:897–907.
[39] Freedman RB, Radda GK. The reaction of 2, 4, 6-trinitrobenzenesulphonic acid with amino acids, peptides and proteins. Biochem J 1968;108:383–91.
[40] Bir K, Crawhall JC, Mauldin D. Reduction of disulfides with sodium and potassium borohydrides and its application to urinary disulfides. Clin Chim Acta 1970;30:183–90.
[41] Köping-Höggård M, Vårum KM, Issa M, Danielsen S, Christensen BE, Stokke BT, et al. Improved chitosan-mediated gene delivery based on easily dissociated chitosan polyplexes of highly defined chitosan oligomers. Gene Ther 2004;11:1441–52.
[42] Lepecq JB, Paoletti C. A fluorescent complex between ethidium bromide and nucleic acids: Physical—Chemical characterization. J Mol Biol 1967;27:87–106.
[43] Mahmoodi M, Behzad-Behbahani A, Sharifzadeh S, Abolmaali SS, Tamaddon A. Co-condensation synthesis of well-defined mesoporous silica nanoparticles: Effect of surface chemical modification on plasmid DNA condensation and transfection. IET Nanbiotechnol 2017;11:995–1004.
[44] Gerlier D, Thomasset N. Use of MTT colorimetric assay to measure cell activation. J Immunol Methods 1986;94:57–63.
[45] Strober W. Trypan blue exclusion test of cell viability. Curr Protoc Immunol 2001;21(1):A.3B.1–A.3B.2.
[46] Ciniglia C, Pinto G, Sansone C, Pollio A . Acridine orange/Ethidium bromide double staining test: a simple *in vitro* assay to detect apoptosis induced by phenolic compounds in plant cells. Allelopathy J 2010;26:301–8.
[47] Santos JL, Pandita D, Rodrigues J, Pêgo AP, Granja PL, Balian G, et al. Receptor-mediated gene delivery using PAMAM dendrimers conjugated with peptides recognized by mesenchymal stem cells. Mol Pharmaceut 2010;7:763–74.
[48] Snyder SL, Sobocinski PZ. An improved 2, 4, 6-trinitrobenzenesulfonic acid method for the determination of amines. Anal Biochem 1975;64:284–8.
[49] Stocks SJ, Jones AJM, Ramey CW, Brooks DE. A fluorometric assay of the degree of modification of protein primary amines with polyethylene glycol. Anal Biochem 1986;154:232–4.
[50] Abolmaali SS, Tamaddon AM, Kamali-Sarvestani E, Ashraf MJ, Dinarvand R. Stealth nanogels of histinylated poly ethyleneimine for sustained delivery of methotrexate in collagen-induced arthritis. Model Pharm Res 2015;32(10):3309–23.
[51] Dehshahri A, Oskuee RK, Shier WT, Hatefi A, Ramezani M. Gene transfer efficiency of high primary amine content, hydrophobic, alkyl-oligoamine derivatives of polyethylenimine. Biomaterials 2009;30:4187–94.
[52] Sundberg RJ, Martin RB. Interactions of histidine and other imidazole derivatives with transition metal ions in chemical and biological systems. Chem Rev 1974;74:471–517.
[53] Soshilov AA, Denison MS. DNA binding (gel retardation assay) analysis for identification of aryl hydrocarbon (Ah) receptor agonists and antagonists. In: Caldwell GW, Yan ZY, editors. Optimization in drug discovery: *in vitro* methods. Totowa, NJ: Humana Press; 2014. p. 207–19.
[54] Scott V, Clark AR, Docherty K. The gel retardation assay. In: Harwood AJ, editor. Protocols for gene analysis. Totowa, NJ: Humana Press; 1994. p. 339–47.
[55] Golkar N, Samani SM, Tamaddon AM. Cholesterol-conjugated supramolecular assemblies of low generations polyamidoamine dendrimers for enhanced EGFP plasmid DNA transfection. J Nanopart Res 2016;18:107.
[56] Hartlieb M, Pretzel D, Kempe K, Fritzsche C, Paulus RM, Gottschaldt M, et al. Cationic poly (2-oxazoline) hydrogels for reversible DNA binding. Soft Matter 2013;9:4693–704.
[57] Kleemann E, Neu M, Jekel N, Fink L, Schmehl T, Gessler T, et al. Nano-carriers for DNA delivery to the lung based upon a TAT-derived peptide covalently coupled to PEG–PEI. J Control Release 2005;109:299–316.
[58] Tavakoli S, Tamaddon AM, Golkar N, Samani SM. Microencapsulation of (deoxythymidine) 20–DOTAP complexes in stealth liposomes optimized by Taguchi design. J Liposome Res 2015;25:67–77.
[59] Geall AJ, Blagbrough IS. Rapid and sensitive ethidium bromide fluorescence quenching assay of polyamine conjugate–DNA interactions for the analysis of lipoplex formation in gene therapy. J Pharm Biomed Anal 2000;22:849–59.
[60] Zintchenko A, Philipp A, Dehshahri A, Wagner E. Simple modifications of branched PEI lead to highly efficient siRNA carriers with low toxicity. Bioconjug Chem 2008;19:1448–55.
[61] Fischer D, Bieber T, Li Y, Elsässer HP, Kissel T. A novel non-viral vector for DNA delivery based on low molecular weight, branched polyethylenimine: Effect of molecular weight on transfection efficiency and cytotoxicity. Pharm Res 1999;16:1273–9.
[62] Zheng N, Song Z, Liu Y, Zhang R, Zhang R, Yao C, et al. Redox-responsive, reversibly-crosslinked thiolated cationic helical polypeptides for efficient siRNA encapsulation and delivery. J Control Release 2015;205:231–9.
[63] Venault A, Huang YC, Lo JW, Chou CJ, Chinnathambi A, Higuchi A, et al. Tunable PEGylation of branch-type PEI/DNA polyplexes with a compromise of low cytotoxicity and high

transgene expression: *In vitro* and *in vivo* gene delivery. J Mater Chem B 2017;5:4732–44.
[64] Brunot C, Ponsonnet L, Lagneau C, Farge P, Picart C, Grosgogeat B. Cytotoxicity of polyethyleneimine (PEI), precursor base layer of polyelectrolyte multilayer films. Biomaterials 2007;28:632–40.
[65] Malik N, Wiwattanapatapee R, Klopsch R, Lorenz K, Frey H, Weener JW, et al. Dendrimers: Relationship between structure and biocompatibility *in vitro*, and preliminary studies on the biodistribution of 125I-labelled polyamidoamine dendrimers *in vivo*. J Control Release 2000;65:133–48.
[66] Fischer D, Li Y, Ahlemeyer B, Krieglstein J, Kissel T. *In vitro* cytotoxicity testing of polycations: influence of polymer structure on cell viability and hemolysis. Biomaterials 2003;24:1121–31.
[67] Louis KS, Siegel AC. Cell viability analysis using trypan blue: Manual and automated methods. Mammalian cell viability. Springer; 2011. p. 7–12.
[68] Gao S, Tian H, Guo Y, Li Y, Guo Z, Zhu X, et al. miRNA oligonucleotide and sponge for miRNA-21 inhibition mediated by PEI-PLL in breast cancer therapy. Acta Biomater 2015;25:184–93.
[69] Zhi F, Dong H, Jia X, Guo W, Lu H, Yang Y, et al. Functionalized graphene oxide mediated adriamycin delivery and miR-21 gene silencing to overcome tumor multidrug resistance *in vitro*. Plos One 2013;8:e60034.
[70] Foged C, Brodin B, Frokjaer S, Sundblad A. Particle size and surface charge affect particle uptake by human dendritic cells in an *in vitro* model. Int J Pharm 2005;298(2):315–22.
[71] Shim MS, Kwon YJ. Efficient and targeted delivery of siRNA *in vivo*. FEBS J 2010;277:4814–27.
[72] Drayton RM. The role of microRNA in the response to cisplatin treatment. Portland Press Limited; 2012.
[73] Eitan R, Kushnir M, Lithwick-Yanai G, David MB, Hoshen M, Glezerman M, et al. Tumor microRNA expression patterns associated with resistance to platinum based chemotherapy and survival in ovarian cancer patients. Gynecol Oncol 2009;114:253–9.
[74] Titone R, Morani F, Follo C, Vidoni C, Mezzanzanica D, Isidoro C. Epigenetic control of autophagy by microRNAs in ovarian cancer. Biomed Res Int 2014;2014:343542.
[75] Bourguignon LYW. Overcoming chemotherapy resistance by targeting hyaluronan/cd44-mediated stem cell marker (nanog) signaling and microrna-21 in breast, ovarian, and head and neck cancer. In: Hayat, editor. Stem cells and cancer stem cells, volume 9: Therapeutic application in disease and injury. Dordrecht: Springer; 2013. p. 291–8.